Electrochimica Acta 394 (2021) 139107

Contents lists available at ScienceDirect

Electrochimica Acta

journal homepage: www.elsevier.com/locate/electacta

The adsorption of perchlorate, sulfate, selenate and water on Au(111)-textured electrodes from aqueous solutions: Simultaneous voltammetric, optical and microgravimetric studies

Jonathan R. Strobl, Daniel Scherson*

Department of Chemistry, Case Western Reserve University, Cleveland, OH 44106-7078, United States

ARTICLE INFO

Article history:
Received 21 June 2021
Revised 10 August 2021
Accepted 12 August 2021
Available online 19 August 2021

Keywords:
Adsorption
EQCM
Electroreflectance
Perchlorate
Sulfate

ABSTRACT

The adsorption of perchlorate, $ClO_4^-(aq)$, sulfate, $SO_4^{2-}(aq)$ and selenate, $SeO_4^{2-}(aq)$ on Au(111)-textured single crystals from aqueous acidic solutions was examined as a function of the applied potential, E, by simultaneous voltammetry, normal incidence differential reflectance spectroscopy, $\Delta R/R$, and electrochemical quartz crystal microbalance, EQCM, techniques. In particular, $\Delta R/R$ vs E data collected in pure 0.1 M $HClO_4$ or the same electrolyte containing either 1 mM Na_2SO_4 or 1 mM Na_2SeO_4 could be quantitatively accounted for by using a simple model introduced in similar studies reported earlier in this laboratory. This model regards the $\Delta R/R$ response as arising from a sum of contributions from bare and adsorbate covered areas of the surface, which are, in each case, linear functions of the applied potential. Adsorption isotherms for $ClO_4^-(aq)$, and $SO_4^{2-}(aq)$ on Au(111) from the literature allowed fitting of the model to data obtained in 1 mM Na_2SO_4 in 0.1 M $HClO_4$ solutions. The two oxyanions were found to co-adsorb over a wide potential range, with $SO_4^{2-}(aq)$ fully displacing $ClO_4^-(aq)$ for $E > 1.25$ V vs RHE. Analogous $\Delta R/R$ measurements involving 1 mM Na_2SeO_4 in 0.1 M $HClO_4$ solutions combined with the model allowed calculation of the coverage of the two oxyanions as a function of E. The experimental isotherms enabled calculation of the mass densities for the adsorbed oxyanions, ρ_{th}, yielding values virtually identical to those derived from EQCM experiments, ρ_{exp}, for data recorded in the range ca. $E < 0.73$ V vs RHE in all three solutions. At higher potentials, however, ρ_{exp} were significantly larger than those predicted by the optical measurements, a behavior consistent with water co-adsorption.

1. Introduction

Considerable efforts have been made over the past few decades toward the development of highly specific and sensitive methods for monitoring in real time the adsorption of neutral and ionic species on well-defined electrode surfaces. Particularly promising, because of their unparalleled time resolution, are optical techniques. However, the fundamental physics that govern the optical response of metal surfaces are very complex, a factor that has so far limited their practical utility in the study of quantitative interfacial dynamics in general. Nevertheless, empirical correlations have been found in our laboratory between differential reflectance, $\Delta R/R$ [1–3] and second harmonic generation, SHG [3], and the actual coverage, θ, of simple species as determined from interfacial thermodynamic analyses, radiochemical or spectroscopic techniques. For a review article in the area of reflectance spectroscopy as applied to electrochemical systems see Ref. [4]. As detailed in our earlier publications [1,2], remarkable agreement with the optical results could be obtained by assuming $\Delta R/R$ arises from additive contributions derived from the bare and adsorbate covered surface fractions, namely,

$$\Delta R/R = A(E)\left(1 - \theta_X/\theta_X^{sat}\right) + B(E)\left(\theta_X/\theta_X^{sat}\right) \quad (1)$$

where θ_X is the potential dependent coverage of a given adsorbed species, X, and θ_X^{sat} its saturation value, and $A(E)$ and $B(E)$ are linear functions of the applied potential, E, that represent, respectively, the intrinsic electroreflectance for the adsorbate-free surface ($\theta_X = 0$) and the intrinsic electroreflectance for the adsorbate saturated surface ($\theta_X = \theta_X^{sat}$). Of note, all coverages in this paper represent the ratio of the adsorbate density to the Au(111) surface atom density. Indeed, Eq. (1) could quantitatively account for $\Delta R/R$ data collected for the adsorption of $SO_4^{2-}(aq)$, hydrogen and a few other species on quasi perfect Pt(111) facets in acidic aqueous electrolytes [1,3], using values of θ_X as a function of potential determined from independent measurements. Prompted by the recent discovery of the electrocatalytic properties of underpotential deposited Cu on Au to promote the rates of selenate, $SeO_4^{2-}(aq)$,

* Corresponding author.
E-mail address: dxs16@case.edu (D. Scherson).

https://doi.org/10.1016/j.electacta.2021.139107
0013-4686/

reduction in aqueous acidic solutions [5], we embarked on a series of studies involving simultaneous acquisition of electrochemical, $\Delta R/R$, and microgravimetric data on highly textured Au(111) films supported on a quartz crystal microbalance, using a modified commercial cell similar to that developed in our earlier studies [6]. The primary aim of this investigation was not only to assess the ability of Eq. (1) to quantitatively account for the $\Delta R/R$ response to anion adsorption on Au(111) in $ClO_4^-(aq)$, $SO_4^{2-}(aq)$ and $SeO_4^{2-}(aq)$ containing solutions, but also to determine the adsorption isotherm for SeO_4^{2-} on Au(111), which will be relevant in future studies of its electrocatalytic reduction.

In particular, values of $\theta_{ClO_4^-}$ calculated from the adsorption isotherm for $ClO_4^-(aq)$ reported by Zhumaev et al. based on surface enhanced infrared absorption spectroscopy, SEIRAS [7], were used to determine best fit parameters for *A(E)* and *B(E)* in Eq. (1), yielding excellent agreement with $\Delta R/R$ vs E data collected in 0.1 M $HClO_4$. This information, in addition to surface excesses for SO_4^{2-} determined from thermodynamic analyses and radiochemical measurements [8], were then employed to analyze $\Delta R/R$ data collected in mixed $ClO_4^-(aq)$, and $SO_4^{2-}(aq)$ containing solutions. The results obtained allowed the surface composition to be determined as a function of E, affording strong evidence for the co-adsorption of both ions over a substantial range of potentials, a phenomenon that has not been reported in the literature. In addition, application of this optical model to data collected in mixed $ClO_4^-(aq)$ and $SeO_4^{2-}(aq)$ electrolytes made it possible to derive adsorption isotherms for co-adsorbed ClO_4^- and SeO_4^{2-}, information not previously available in the literature.

Lastly, insight into the coverages of adsorbed water at these interfaces was gained by comparing anion mass densities derived from the isotherms, ρ_{th}, with experimental mass densities, ρ_{exp}, determined from electrochemical quartz crystal microbalance, EQCM, measurements. The excess mass was attributed to co-adsorbed water molecules and appeared over the same potential ranges as SEIRAS modes for adsorbed water reported in perchloric and sulfuric acid solutions [9,10]. Overall, the ability to monitor $\Delta R/R$ and the EQCM frequency simultaneously offers unparalleled insights when attempting to determine anion and water co-adsorption as a function of the applied potential, providing information not available with each independent technique.

2. Experimental section

Most of the measurements were performed with a commercial PVDF EQCM cell (Metrohm), which was modified in our laboratory to allow simultaneous *in situ* optical experiments to be performed (see Fig. 1 and caption for details). Perchloric acid (EMD Millipore, Omnitrace, 65–71%), Na_2SO_4 (Fisher Scientific, anhydrous, certified ACS), and $Na_2SeO_4 \cdot 10H_2O$ (Alfa Aesar, 99.9%) were used to prepare solutions for all experiments. The $Na_2SeO_4 \cdot 10H_2O$ was purified using the method published by Gruebel et al. [11] Specifically, a 0.2 M Na_2SeO_4 + 0.1 M $HClO_4$ stock solution was stirred for more than 10 h with a 30 g/L suspension of TiO_2 (Sigma Aldrich, rutile, 99.98%) and the TiO_2 adsorbent filtered to remove H_2SeO_3(aq) impurities adsorbed on the TiO_2 surface. This procedure was performed three times, yielding a $SeO_4^{2-}(aq)$- containing solution devoid of any detectable selenite, $SeO_3^{2-}(aq)$. All solutions were prepared using UPW generated by a Barnstead Micropure UV/UF filtration system and purged with Ar (PP300, Airgas) prior to each electrochemical experiment.

Normal incidence differential reflectance (NIDR) measurements were performed using an optical arrangement similar to that described in a previous publication [2]. Specifically, light from a 632.8 nm HeNe laser (2 mW, Thor Labs, HNL020RB) was passed through a linear polarizer and split by a beam splitter, allowing 50% of the light to reach a reference detector (DET10A Si based detector, Thor Labs), while the other 50% was reflected off the surface of the working electrode at normal incidence and directed to a second identical or 'sample' detector. As is customary, the data will be displayed as $(\Delta R/R)^{632} = [R(E) - R(E_{ref})]/R(E_{ref})$, where, in this case, $R(E) = R'(E,t)/R''(t)$, where *R'(E,t)* is the time dependent intensity of the beam measured at the sample detector at any potential *E*, and *R"(t)* is the intensity of the beam at the reference detector, which is potential independent. In this fashion, it became possible to eliminate temporal drifts in laser power and thus in the $\Delta R/R$ data. The reference potential, E_{ref}, is an arbitrarily selected potential where there are no adsorbed species present on the surface, except possibly water. Unless otherwise specified, E_{ref} = 0.0 V vs RHE. For these experiments, the sample and reference photodiode signals were recorded using a National Instruments USB-6009 Data Acquisition card with a custom LabView program. Data was sampled at 6000 points per s and subjected to boxcar averaging to improve signal to noise.

Microgravimetric measurements, $\Delta f = f(E) - f(E_{ref})$, where f is the resonance frequency of the EQCM, and E_{ref} an arbitrary reference potential, were carried out with an Autolab EQCM module. Unless otherwise specified, E_{ref} = 0.0 V vs RHE, a potential where there are no adsorbed species on the electrode surface. The 6 MHz Au electrodes (Metrohm) were found to display a high degree of Au(111) character and will be referred to hereafter as Au(111)-textured electrodes. Both $\Delta R/R$ and Δf data were collected during repetitive potential cyclings, which were then averaged.

Experiments involving a massive Au(111) crystal (vide infra), were conducted in a custom-made all-glass cell with a Teflon lid, which housed a graphite rod as the counter electrode, CE, and a glass bodied home-made hydrogen-bubble reversible hydrogen electrode, RHE, in the same solution [12], separated from the working electrode compartment by a Vycor frit, as a reference electrode, RE. Prior to use, this cell was cleaned by soaking in piranha solution (10:1 concentrated H_2SO_4:30% H_2O_2 in water) followed by thorough rinsing and subsequent boiling in UPW, a minimum of 4 times. *Piranha solution is extremely corrosive and oxidizing and must be handled with extreme caution using appropriate PPE*. The Au(111) crystal was a solid cylinder with its main axis oriented normal to the face of interest, which was thoroughly flame-annealed in a propane/air flame prior to use.

For all experiments, the potential of the electrodes was controlled with an Autolab PGSTAT302N potentiostat.

3. Results and discussion

3.1. Adsorption of perchlorate on Au(111) in 0.1 M $HClO_4$

Shown in Fig. 2 are the cyclic voltammogram (ν = 0.1 V/s, Panel A), averaged EQCM frequency shifts (see caption for details), $\Delta f = f(E) - f(E_{ref})$ (Panel B), and normalized differential reflectance $(\Delta R/R)^{632} = [R(E) - R(E_{ref})]/R(E_{ref})$ (λ = 632 nm, Panel C, E_{ref} = 0.0 V), vs E, recorded with a Au(111)-textured electrode in 0.1 M $HClO_4$.

Also displayed in Panel A in this figure (see red curve, right ordinate), is a plot of the adsorption isotherm for ClO_4^- reported by Zhumaev et al. for Au(111) in the same electrolyte [7], based on the integrated peak areas of the characteristic asymmetric (Cl-O) stretching band, ν_{asym}, in their SEIRAS measurements, namely,

$$Ka_{ClO_4^-} \exp\left(\frac{\gamma F \Delta E}{RT}\right) = \frac{\theta_{ClO_4^-}/\theta^{sat}_{ClO_4^-}}{r\left(1 - \theta_{ClO_4^-}/\theta^{sat}_{ClO_4^-}\right)^r} \quad (2)$$

where K is a constant, $a_{ClO_4^-}$ the activity of $ClO_4^-(aq)$, γ its electrosorption valency, $\Delta E = E - E^o$, r is the number of solvent

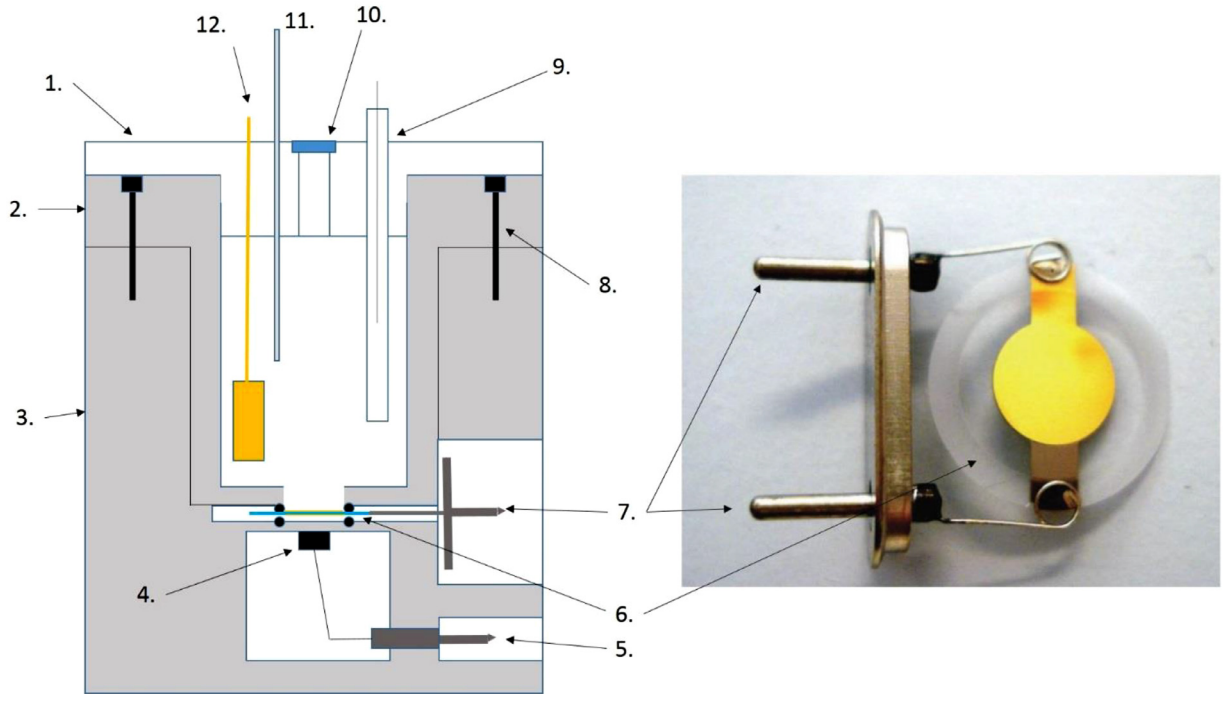

Fig. 1. Cross sectional side view of the cell used for EQCM/NIDR experiments (left), with a top down picture of the working electrode at right. Labeled parts are as follows: 1. Teflon lid, bearing holes drilled for electrodes and a central window to admit the laser beam into the cell for $\Delta R/R$ measurements. 2. Cell body, top half, made of PVDF. 3. Cell body, bottom, made of PVDF. 4. Thermocouple mounted beneath the EQCM electrode (6). 5. Electrical contact for thermocouple. 6. Au coated EQCM electrode, held in place by o-rings (black circles). 7. Electrical contact for top/bottom pad of the EQCM electrode. 8. Screw holding top and bottom halves of cell body together. 9. H_2-bubble RHE reference electrode constructed from Pt wire sealed inside of a glass tube. 10. Fused silica window. 11. Thin Teflon tube for purging electrolyte with inert gas. 12. Au foil counter electrode and Au wire contact.

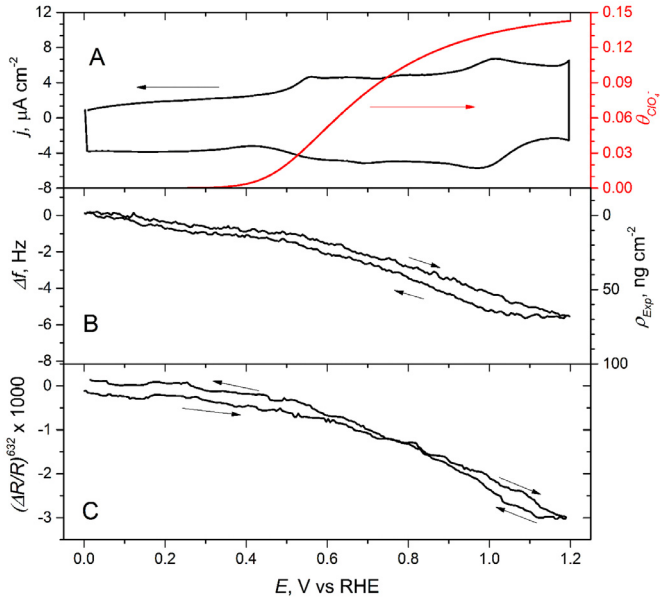

Fig. 2. Cyclic voltammogram (ν = 0.1 V/s, black line, Panel A), averaged EQCM frequency shifts Δf (Panel B), and $(\Delta R/R)^{632}$ (Panel C, E_{ref} = 0.0 V) vs. E, recorded simultaneously with a Au(111)-textured electrode in 0.1 M $HClO_4$ as a function of the applied potential, *E*. The EQCM and optical responses represent the co-added average of 5 and 27 scans, respectively. Also included in Panel A in this figure is a plot of the adsorption isotherm for $ClO_4^-(aq)$ reported by Zhumaev et al. for Au(111) in the same electrolyte [7] (red line, see text for details).

molecules displaced on adsorption, and other symbols have their usual significance. The actual values for these parameters are listed in Table 1. The original version of Eq. (2) from Zhumaev's paper expressed the coverage as a fraction of the saturation coverage,

Table 1
Adsorption isotherm parameters for $ClO_4^-(aq)$ on Au(111) in 0.1 M $HClO_4$ reported by Zhumaev et al. [7]

Symbol	Parameter Values
K	0.35
$a_{ClO_4^-}$	0.08
γ	0.60
r	5
E^0	0.47 V vs RHE
$\theta^{sat}_{ClO_4^-}$	0.15

i.e. $\theta_{Zh} = \theta_{ClO_4^-}/\theta^{sat}_{ClO_4^-}$, whereas Eq. (2) above expresses the same isotherm in terms of $\theta_{ClO_4^-}$, i.e. the ratio of $ClO_4^-(ads)$ density to the surface atom density of Au(111), $d_{Au(111)}$ =2.31 nmol Au/cm^2. Based on their coulometric analysis, these authors estimated a value of $\theta^{sat}_{ClO_4^-}$ of ca. 0.15, which is a bit lower than that found for sulfate, $\theta^{sat}_{SO_4^{2-}}$ = 0.2, using scanning tunneling microscopy [13], STM, but identical to the $\theta^{sat}_{ClO_4^-}$ reported by Ataka et al. [9].

The values of $\theta_{ClO_4^-}$ determined from Eq. (2) and Table 1 were used to find best fit parameters for our primitive model, Eq. (1), written in a more explicit form in Eq. (3) below, to the $(\Delta R/R)^{632}$ signal measured for Au(111) in 0.1 M $HClO_4$.

$$(\Delta R/R)^{632} = (m_1E + b_1)(\theta_{ClO_4^-}/\theta^{sat}_{ClO_4^-}) + (m_2E + b_2)\left(1 - \theta_{ClO_4^-}/\theta^{sat}_{ClO_4^-}\right) \quad (3)$$

Least squares fitting of Eq. (3) to the experimental $(\Delta R/R)^{632}$ results in 0.1 M $HClO_4$ (see blue curve in Fig. 3) yielded best fit m_1, b_1, m_2 and b_2 values (see caption Fig. 3), which accurately reproduced the observed behavior (see scattered black symbols in

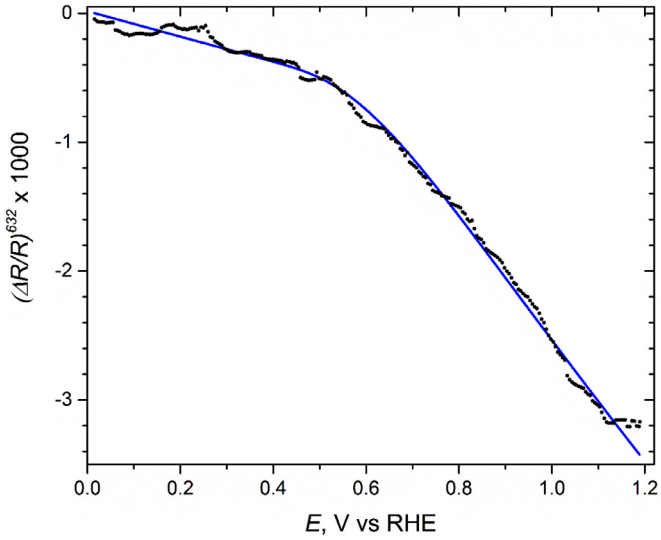

Fig. 3. Plot of $(\Delta R/R)^{632}$ vs. E (scattered black symbols) recorded for scans toward negative potentials for a Au(111)-textured surface in 0.1 M $HClO_4$ in the EQCM cell. These data represent an average of 27 co-added scans recorded at a rate of $\nu = 0.1$ V/s, whereas the blue line is the best fit to the experimental data based on Eq. (3). Best fit parameters are as follows: m_1 = -4.21 × 10^{-3}/V, b_1 = 1.46 × 10^{-3}, m_2 = -9.89 × 10^{-4}/V, and b_2 = 1.62 × 10^{-5}.

Fig. 3). As predicted by our model, the $\Delta R/R$ signal is linear in E prior to the onset of ClO_4^- adsorption at $E = 0.4$ V, whereas above 0.4 V, the signal bends downwards and adopts a steeper slope that is proportional to $\theta_{ClO_4^-}$.

Additional insight into the role of water in the $ClO_4^-(ads)$ layer could be obtained from simultaneous microgravimetric measurements shown in Panel B, Fig. 2. Particularly puzzling is the increase in the mass observed for potentials negative to the onset of $ClO_4^-(aq)$adsorption, i.e. $E < 0.32$ V, although water is the most likely species responsible for this behavior. The Δf vs E values collected for $E > 0.32$ V were used to construct a plot of the mass density determined from EQCM, ρ_{exp}, using the Sauerbrey equation below,

$$\rho_{exp} = -\Delta f \sqrt{\rho_{quartz}\mu_{quartz}}/2{f_0}^2 \quad (4)$$

where f_0 is the fundamental frequency of the EQCM crystal (6 MHz), $\rho_{quartz}$is the density of quartz (2.648 g/cm^3), and μ is its shear modulus (2.947 × 10^{11} g cm^{-1} s^{-2}), against the mass density of desolvated $ClO_4^-(ads)$, ρ_{th}, determined from Eq. (5) below

$$\rho_{th} = \theta_{ClO_4^-} \cdot M_{ClO_4^-} \cdot d_{Au(111)} \quad (5)$$

where $\theta_{ClO_4^-}$is taken from Eq. (2), $M_{ClO_4^-}$ = 99.45 g/mol, and $d_{Au(111)}$, the density of Au surface atoms, is 2.31 nmol/cm^2. This is shown in Fig. 4. Also shown by the black line in this figure is a linear fit to the data for values of ρ_{exp} in the range 0 up to about 20 nm/cm^2 (which corresponds to a potential range 0.365 V < E < 0.74 V), yielding a slope of 1.03 and an intercept of 0. The very close agreement between these two mass densities indicates that the mass change for this potential range is dominated by the adsorption of desolvated ClO_4^-. As clearly seen in the figure, this remarkable correlation deviated significantly for $\rho_{exp} > 21$ nm/cm^2 affording evidence for monotonic increases in the mass well exceeding those of a fully desolvated ion, which suggest an increase of the degree of anion solvation.

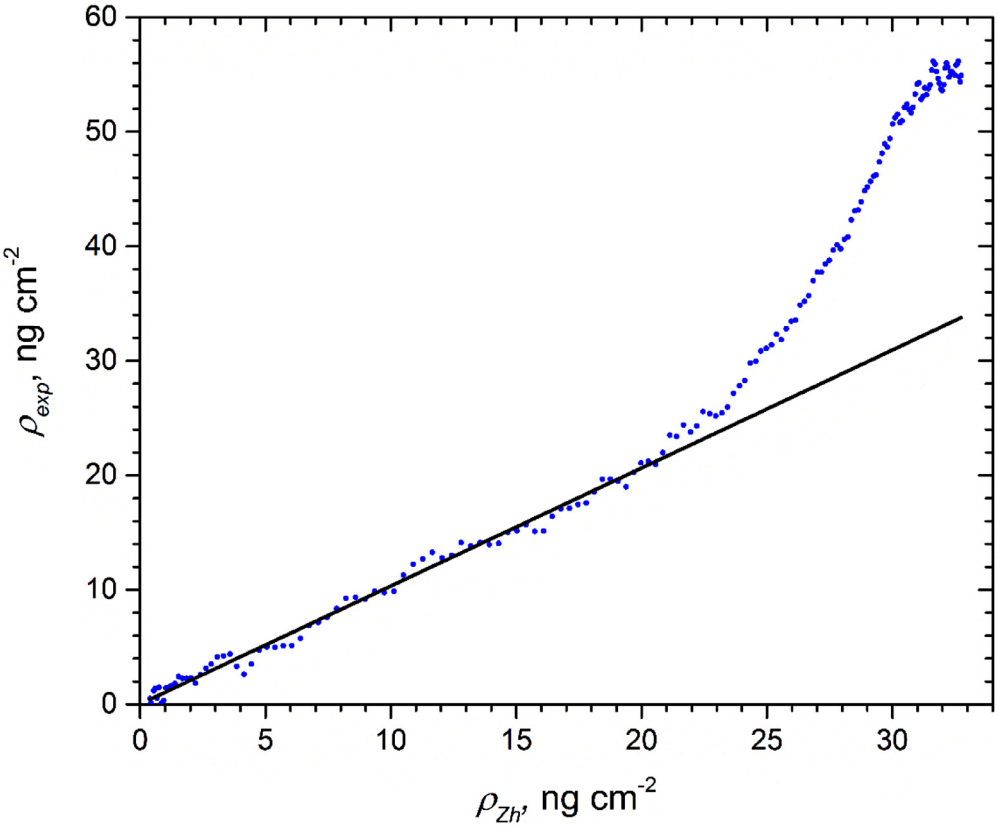

Fig. 4. Plot of the mass density measured via EQCM in 0.1 M $HClO_4$ during a 0.1 V/s scan in the negative direction, ρ_{exp},referenced to a mass of zero at $E = 0.365$ V, against the mass of $ClO_4^-(ads)$ calculated from the isotherm reported by Zhumaev et al. [7] assuming the adsorbed ion is fully desolvated, ρ_{th}. The black line is the best linear fit to the data for values of $\rho_{exp} \leq 21$ ng/cm^2, which correspond to a potential range 0.365 V < E < 0.74 V. Least squares fit function: $\rho_{exp} = 1.03 \times \rho_{th}$.

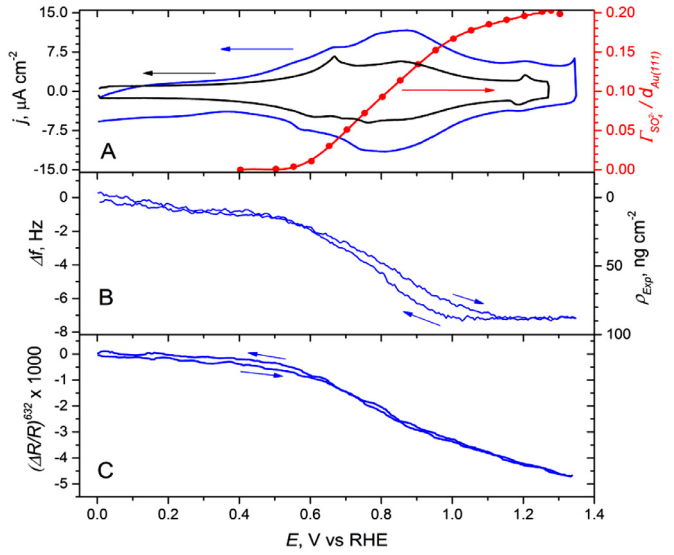

Fig. 5. Cyclic voltammogram (ν = 0.1 V/s, blue line, Panel A), Δf (average of 5 scans, E_{ref} = 0.0 V) as measured with EQCM (Panel B), and $(\Delta R/R)^{632}$ (average of 27 scans, Panel C, E_{ref} = 0.0 V) recorded simultaneously with a Au(111)-textured EQCM electrode in 0.1 M $HClO_4$ with 1 mM Na_2SO_4 as a function of the applied potential. Also included in Panel A is a voltammogram recorded with a massive Au(111) single crystal (ν = 0.05 V/s, black line) and a plot of the surface excess for SO_4^{2-} reported by Shi et al. [8] for Au(111) in 1 mM K_2SO_4 in 0.1 M $HClO_4$ (red points, right ordinate), which has been normalized by $d_{Au(111)}$, where the solid red line is a high order polynomial fit to the data, generated for interpolation purposes.

As clearly evident in Fig. 4, ρ_{exp} is nearly equal to $\rho_{Zh}$for 0.365 V < E < 0.74 V, if we assume perchlorate adsorption induces no net co-adsorption or displacement of interfacial water. However, in their original publication [7], Zhumaev et al. asserted that the adsorption of a single perchlorate ion would trigger the net displacement of 5 interfacial water molecules, which would reduce the effective molar mass per adsorbed perchlorate from 99.45 to 9.38 g/mol. This is clearly inconsistent with the ρ_{exp} reported here. As such, it seems that even though Eq. (3) accurately fits the $\theta_{ClO_4^-}$ vs. E trend, it does not properly describe the amount of co-adsorbing/displaced water, which, as indicated by our results, varies with the potential.

3.2. Co-adsorption of Perchlorate and Sulfate on Au(111) in 1 mM Na_2SO_4 in 0.1 M $HClO_4$

Encouraged by the ability of the primitive model to account for the $\Delta R/R$ response of $ClO_4^-(aq)$ adsorption on Au(111), we decided to explore whether this approach could be extended to the co-adsorption of $ClO_4^-(aq)$ and $SO_4^{2-}(ads)$, where adsorption of the latter has been extensively studied with a variety of techniques including measurements of surface excesses [8,14], radiochemistry [8], STM [13,15,16], infrared absorption spectroscopy [13,17] (IRAS), SEIRAS [10], SHG [14], and surface X-ray scattering (SXS) [18]. Shown in Fig. 5 is the cyclic voltammogram (ν = 0.1 V/s, black line, Panel A), averaged Δf (Panel B), and $(\Delta R/R)^{632}$ (Panel C, E_{ref} = 0.0 V) vs. E, recorded simultaneously with a Au(111)-textured electrode in a 1 mM Na_2SO_4 in 0.1 M $HClO_4$ solution, as a function of E. Also depicted in Panel A in this figure (see black curve) is the cyclic voltammetry of a massive Au(111) crystal recorded in this laboratory in the same electrolyte, which displays features believed to be characteristic of low index face reported by other authors [8,10,13–16,18], which are much sharper compared to those found for the textured Au(111) (see blue curve). As has been amply discussed in the literature, at potentials negative to the current peak centered at about 0.6 V, Au(111) displays a (1 × 23) reconstruction [10], which is lifted at more positive potentials, a process that is quite reversible. The second, and much broader peak centered at ca. 0.8 V, has been associated with the adsorption of $SO_4^{2-}(aq)$ into what has been referred to as a disorganized, 'gas-like' state devoid of any particular order. The lack of any visible STM [13,14] features that could be ascribed to adsorbed ions in the potential range associated with this feature has led some authors to assert that $SO_4^{2-}(ads)$ is highly mobile, i.e. it has low diffusional barriers. The presence of $SO_4^{2-}(ads)$ in this potential range, however, has been confirmed by Shi et al. [8] based on a rigorous thermodynamic analysis and radiochemical methods, and also by infrared reflection absorption, IRAS [13], and SEIRAS [10]. Lastly, the reversible peak at ca. 1.2 V has been ascribed to a rather sudden structural change of the adsorbed ionic layer yielding a rigid, 'solid-like' adlayer of close-packed $SO_4^{2-}(ads)$[13,15], as evidenced by the analysis of STM data. In an early STM study, Magnussen et al. [15] claimed that this adlayer exhibits a saturation coverage, $\theta^{sat}_{SO_4^{2-}} = 0.4$, based on the density of height maxima in the STM images. Later, Edens et al. [13] argued that only one half of these STM peaks actually correspond to $SO_4^{2-}(ads)$, and that the real adlayer structure was a $\sqrt{3}$ x $\sqrt{7}$ R19° lattice of $SO_4^{2-}(ads)$ with $\theta^{sat}_{SO_4^{2-}} = 0.2$, and that the other STM peaks could be attributed to 0.2 of co-adsorbed hydronium cations, arranged between the rows of $SO_4^{2-}(ads)$. In related studies, Ataka and Osawa [10] examined the potential dependent ν_{asym} mode of $SO_4^{2-}(ads)$ Au(111) with SEIRS, and concluded that the mode at 1654 cm^{-1} could be attributed to co-adsorbed water incorporated into the $SO_4^{2-}(ads)$ adlayer. In addition, the maximum SO_4^{2-} surface excesses measured by Shi et al. [8] in 0.1 M $HClO_4$ + X mM K_2SO_4 are were found to be roughly equal to 1/5 of $d_{Au(111)}$ (vide infra). Finally, a SXS analysis by Kondo et al. [18] was consistent with a value of $\theta^{sat}_{SO_4^{2-}} = 0.22$.

Also included in Panel A in Fig. 5 is a plot of the adsorption isotherm for SO_4^{2-} reported by Shi et al. [8] for Au(111) in the same electrolyte (red line). This mixed perchlorate / sulfate electrolyte is particularly interesting, as the onset of $ClO_4^-(aq)$ adsorption in 0.1 M $HClO_4$, occurs at a potential negative to the reported onset of $SO_4^{2-}(aq)$ adsorption from 1 mM sulfate solutions in the same electrolyte. While the data published in the literature affords rather unambiguous evidence that $SO_4^{2-}(ads)$ will saturate the surface at high potentials, thereby fully displacing $ClO_4^-(ads)$, it seems likely, and indeed reasonable, that for small $\theta_{SO_4^{2-}}$, there may still be some co-adsorbed ClO_4^- on the surface, which would thus contribute to both the ΔR/R and microgravimetric signals. Support for this proposal can be gleaned from Panel C, Fig. 5, wherein the $(\Delta R/R)^{632}$ response in 0.1 M $HClO_4$ + 1 mM Na_2SO_4 curves downwards starting at around 0.4 V, i.e. ca. 150 mV negative of the onset of $SO_4^{2-}(aq)$ adsorption. Eq. (1) predicts that $(\Delta R/R)^{632}$ will depend linearly on E for a fixed θ_X and only curve as θ_X varies. Indeed, as shown in Panel A, Fig. 2, the onset of downwards curvature aligns closely with the onset of ClO_4^- adsorption reported by Zhumaev et al. [7].

Our proposed extended primitive model (see Eq. (6)) regards $(\Delta R/R)^{632}$ in 1 mM Na_2SO_4 in 0.1 M $HClO_4$ as arising from additive contributions due to $\theta_{SO_4^{2-}}$, the fraction of the surface covered by SO_4^{2-}, and $1 - \frac{\theta_{SO_4^{2-}}}{\theta^{sat}_{SO_4^{2-}}}$, the corresponding fraction of uncovered and ClO_4^-–covered sites, which correspond to the left and right terms in Eq. (6), respectively. Note that the term in curly brackets is precisely $(\Delta R/R)^{632}$obtained in SO_4^{2-}–free, 0.1 M $HClO_4$ solution, (see blue line in Figs. 3 and 6).

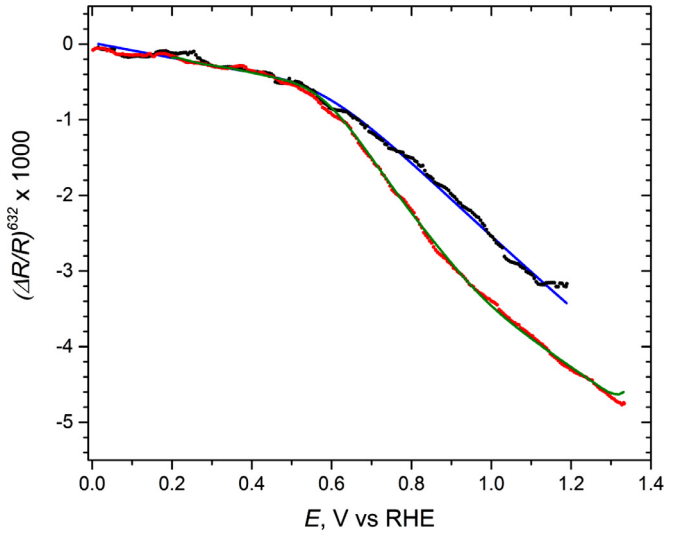

Fig. 6. Plots of $(\Delta R/R)^{632}$ vs E for Au(111) in 0.1 M $HClO_4$ (black line) and 1 mM Na_2SO_4 in 0.1 M $HClO_4$ solutions (red line) acquired during $\nu = 0.1$ V/s scans in the negative direction (average of 27 scans). Also included are best fits the data based on Eq. (3) (blue line) and Eq. (6) (green line). Best fit parameters for Eq. (3) are reported in Fig. 3, whereas those for Eq. (6) are as follows: $m_3 = -3.22 \times 10^{-3}$/V, $b_3 = -4.22 \times 10^{-4}$.

$$(\Delta R/R)^{632}_{mix} = (m_3E + b_3)\cdot\frac{\theta_{SO_4^{2-}}}{\theta^{sat}_{SO_4^{2-}}} + \left\{(m_1E + b_1)\frac{\theta_{ClO_4^-}}{\theta^{sat}_{ClO_4^-}} + (m_2E + b_2)\left(1 - \frac{\theta_{ClO_4^-}}{\theta^{sat}_{ClO_4^-}}\right)\right\} \times \left(1 - \frac{\theta_{SO_4^{2-}}}{\theta^{sat}_{SO_4^{2-}}}\right) \quad (6)$$

It becomes evident from this expression that the terms inside the curly brackets will dominate $(\Delta R/R)^{632}_{mix}$ at potentials negative enough for $\theta_{SO_4^{2-}}$ to become negligible, whereas the first term will dominate for potentials positive enough for $\theta_{SO_4^{2-}}$ to reach saturation, i.e. $\theta^{sat}_{SO_4^{2-}} = 0.2$. This model implicitly assumes that the adsorption of ClO_4^- onto the bare (SO_4^{2-}–free) surface fraction is not affected by the presence of $SO_4^{2-}(ads)$. To test the validity of this simple model, we have used the $\Gamma_{SO_4^{2-}}/d_{Au(111)}$ values reported by Shi et al. [8], using the same conditions as those employed in this study, in place of $\theta_{SO_4^{2-}}$. Shown in Fig. 6 are plots of $(\Delta R/R)^{632}$vs E for Au(111) in 1 mM Na_2SO_4 in 0.1 M $HClO_4$ solutions acquired at $\nu = 0.1$ V/s (scattered red symbols) and the best fit to the data based on Eq. (6) (see green line and text for details). For this fit, values of $\theta_{SO_4^{2-}}$were obtained from a polynomial interpolation of the adsorption isotherm data reported by the aforementioned authors, and the parameters (m_1, m_2, b_1, b_2) extracted from our analysis of the data collected in neat 0.1 M $HClO_4$ discussed above, were used. As can be seen from the green line in Fig. 6, this yielded excellent agreement with the experimental data. The $\Delta R/R$ data is identical to the $SO_4^{2-}(aq)$-free data up to the onset of SO_4^{2-} adsorption at ca. 0.6 V, where the slope increases proportionally to $\theta_{SO_4^{2-}}$, and finally adopts linearity again when $\theta_{SO_4^{2-}}$ reaches saturation.

Given the assumption of non-interaction between the $ClO_4^-(ads)$ and $SO_4^{2-}(ads)$, the coverage of $ClO_4^-(ads)$ in the mixed electrolyte, $\theta^{mix}_{ClO_4^-}$, can be written as:

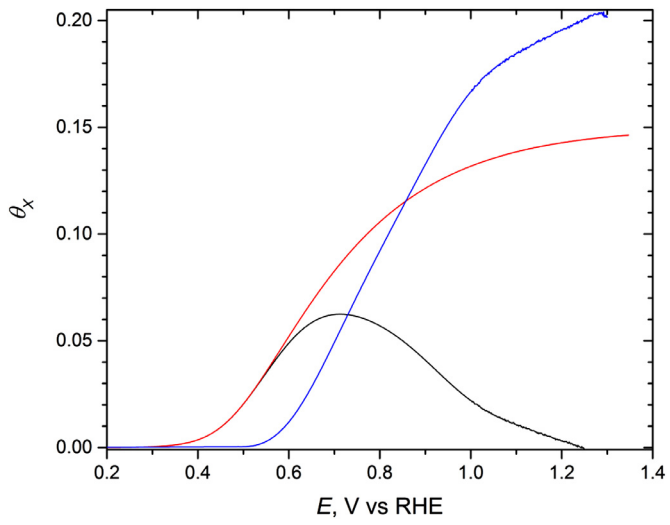

Fig. 7. Plots of $\theta^{mix}_{ClO_4^-}$ vs E for a textured Au(111) electrode in 1 mM Na_2SO_4 in 0.1 M $HClO_4$ solutions (black line), based on the best fit to the experimental data to Eq. (6) and $\theta_{SO_4^{2-}} = \Gamma_{SO_4^{2-}}/d_{Au(111)}$ (blue line), using the surface excesses reported by Shi et al. [8]. Also shown is a plot of $\theta_{ClO_4^-}$ (red line), the coverage of $ClO_4^-(ads)$ on Au(111) in 0.1 M $HClO_4$ vs. E, reported by Zhumaev et al. [7].

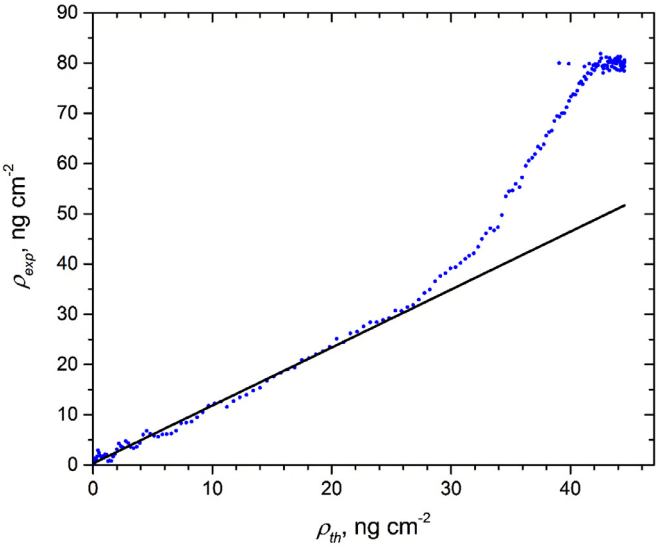

Fig. 8. Plot of $\rho_{exp}$for a Au(111)-textured electrode in 0.1 M $HClO_4$ + 1 mM Na_2SO_4 during a 0.1 V/s scan in the negative direction (referenced to 0 mass at $E = 0.377$ V), vs. the cumulative mass of desolvated, co-adsorbed $ClO_4^-(ads)$ and $SO_4^{2-}(ads)$ based on the data in Fig. 7,ρ_{th}. The black line represents the best linear fit to the data for $\rho_{exp} < 32$ ng/cm^2, i.e. $\rho_{exp} = 1.15 \times \rho_{th}$, which corresponds to that found in the range 0.377 V $< E <$ 0.750 V.

$$\theta^{mix}_{ClO_4^-} = \left(1 - \theta_{SO_4^{2-}}/\theta^{sat}_{SO_4^{2-}}\right) \times \theta_{ClO_4^-} \quad (7)$$

where $\theta_{SO_4^{2-}}$ and $\theta_{ClO_4^-}$ represent, respectively, the $ClO_4^-(ads)$ and $SO_4^{2-}(ads)$ coverages reported by Shi et al. [8], and Zhumaev et al. [7], which makes it possible to plot the surface composition of the Au(111) surface as a function of E (see Fig. 7). As indicated, this model predicts that $\theta^{mix}_{ClO_4^-} = \theta_{ClO_4^-}$ when $\theta_{SO_4^{2-}} = 0$, but decreases gradually to 0 with increasing $\theta_{SO_4^{2-}}$ as the latter approaches saturation.

It is thus of interest to determine whether $\theta_{SO_4^{2-}}$ and $\theta^{mix}_{ClO_4^-}$ vs. E in this figure are consistent with the microgravimetric data collected in 1 mM Na_2SO_4 in 0.1 M $HClO_4$ solutions. Shown in Fig. 8

is a comparison between the experimentally determined mass density, ρ_{exp}, vs the expected mass density extracted from this analysis, ρ_{th} (blue points), i.e.

$$\rho_{th} = (M_{ClO_4^-}\theta^{mix}_{ClO_4^-} + M_{SO_4^{2-}}\theta_{SO_4^{2-}}) \times d_{Au(111)} \quad (8)$$

Rather notably, the data correlates linearly with ρ_{th} up to ρ_{exp} ca. 32 ng/cm^2 (see caption for details), affording a strong indication that the increase in ρ_{exp} is dominated by anion adsorption, and also, that our model accurately predicts this increase. In analogy with the behavior found in 0.1 M $HClO_4$, the data for $\rho_{exp} > 32$ ng/cm^2 ($E > 0.75$ V), deviates quite significantly from linearity. The most likely cause of this effect is water co-adsorption.

The earlier literature does not seem to have considered the possibility of co-adsorption of $ClO_4^-(ads)$ and $SO_4^{2-}(ads)$ on Au(111). In particular, STM [13,15,16] and SXS [18] have been found to be best suited for probing rigid, ordered, solid-like adlayers, which, in the case of a mixed electrolyte, would restrict measurements to be performed at potentials where $SO_4^{2-}(ads)$ is present at close to saturation values, a range in which our results strongly suggest $ClO_4^-(ads)$ would be fully desorbed. Unsurprisingly, no evidence for $ClO_4^-(ads)$ co-adsorption was found by Edens et al. [13] in their STM studies in mixed perchloric/sulfuric acid solutions which yielded images for the saturated SO_4^{2-} adlayer exhibiting the same characteristics as those found in pure sulfuric acid solutions [15,16]. Edens et al. also reported IRAS results in mixed perchloric/sulfuric acid solutions over a wide potential range, including potentials at which $\theta_{SO_4^{2-}}$ would be expected to be well below its saturation value, and attributed the IR peak at 1150–1220 cm^{-1} entirely to $SO_4^{2-}(ads)$ and did not consider perchlorate co-adsorption. It should be noted in this regard, that SEIRAS studies in pure perchloric acid [7,9] and pure sulfuric acid [10] solutions have revealed that the IR features associated with $ClO_4^-(ads)$ and $SO_4^{2-}(ads)$ on Au(111) occur in nearly identical wavenumber regions. Specifically, the SEIRAS spectra reported by Zhumaev et al. [7] in pure perchloric acid solutions displayed an absorption band for $ClO_4^-(ads)$ in the range 1050–1150 cm^{-1}, and thus very similar to that observed by Ataka et al. [9], i.e. 1100–1250 cm^{-1}, in the same electrolyte. In a separate study, Ataka and Osawa [10] reported an IR band for $SO_4^{2-}(ads)$ in pure sulfuric acid solutions at 1155–1195 cm^{-1}. On this basis, it seems unlikely that IR measurements in mixed solutions would be able to resolve the IR bands of $ClO_4^-(ads)$ and $SO_4^{2-}(ads)$. Finally, the SO_4^{2-}surface excesses reported by Shi et al. [8] in mixed perchloric acid/sulfate solutions were calculated from the electrocapillary equation without considering the possibility of perchlorate co-adsorption. However, these authors also determined sulfate coverages via a radiotracer method, and found the results from each method to be consistent. This strongly suggests these authors successfully determined the SO_4^{2-} surface excess at Au(111) in the solutions of interest.

3.3. Co-adsorption of perchlorate and selenate on Au(111) in 1 mM Na_2SeO_4 in 0.1 M $HClO_4$

As mentioned briefly in the Introduction, our interest in the study of the adsorption properties of $SeO_4^{2-}(aq)$ stem from the unique ability of underpotential deposited Cu on Au to catalyze the heterogeneous reduction of this highly inert oxyanion in aqueous acidic electrolytes. As such, we are interested in contrasting the interaction of $SeO_4^{2-}(aq)$ with bare (Cu-free) Au(111), explored in this current work, and Cu UPD covered Au(111), to be explored in a future study. The cyclic voltammetric features, recorded for a massive Au(111) crystal in 1 mM Na_2SeO_4 in 0.1 M $HClO_4$, labeled as A, B and C in the blue curve in Fig. 9 were found to be very similar to those found for 1 mM Na_2SO_4 in the same base electrolyte under

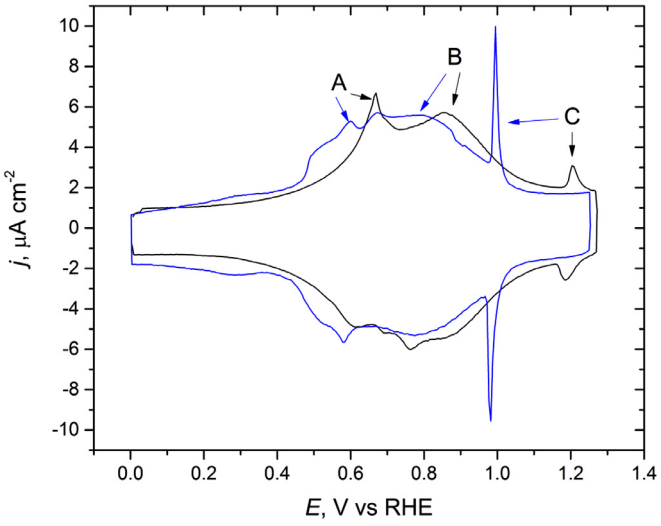

Fig. 9. Cyclic voltammograms (ν = 50 mV/s) for a massive Au(111) electrode recorded in 1 mM Na_2SO_4 (black) or 1 mM Na_2SeO_4 (blue) solutions in 0.1 M $HClO_4$.

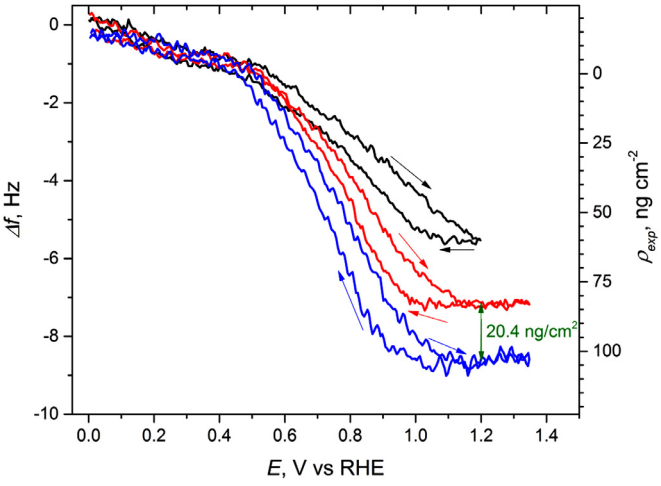

Fig. 10. Plots of Δf vs. E (ν = 0.1 V/s, E_{Ref} = 0 V) collected with a Au(111)-textured electrode in 0.1 M $HClO_4$ before (black curve), and after addition of either 1 mM Na_2SO_4 (red curve) or 1 mM Na_2SeO_4 (blue curve), where the arrows indicate the potential scan direction.

otherwise identical conditions (see black curve in the same figure), and, as such, can be ascribed to the same phenomena discussed in the previous section.

Figure 10 compares EQCM data collected with a Au(111)-textured electrode in neat 0.1 M $HClO_4$ and the same electrolyte with 1 mM Na_2SO_4 or 1 mM Na_2SeO_4. As clearly shown in Fig. 10, each of the ρ_{exp} vs E plots recorded during the negative potential scans display three common regimes:

i a low potential regime where ρ_{exp} is independent of the solution composition, and thus can be ascribed to the behavior of the bare (anion free) surface
ii a middle potential regime at which ρ_{exp} depends rather uniquely on E for each of the oxyanions, and can therefore be attributed to a monotonic increase in the coverage of these species, and
iii a high potential regime, where ρ_{exp} is no longer dependent on E, at which the oxyanions achieve saturation coverage.

The expected mass densities for $\theta = 0.2$ of $SO_4^{2-}(ads)$ and $SeO_4^{2-}(ads)$ on Au(111) are 44.2 and 65.8 ng/cm^2, respectively. The ρ_{exp} plateaus in $SO_4^{2-}(aq)-$, and $SeO_4^{2-}(aq)-$containing solutions

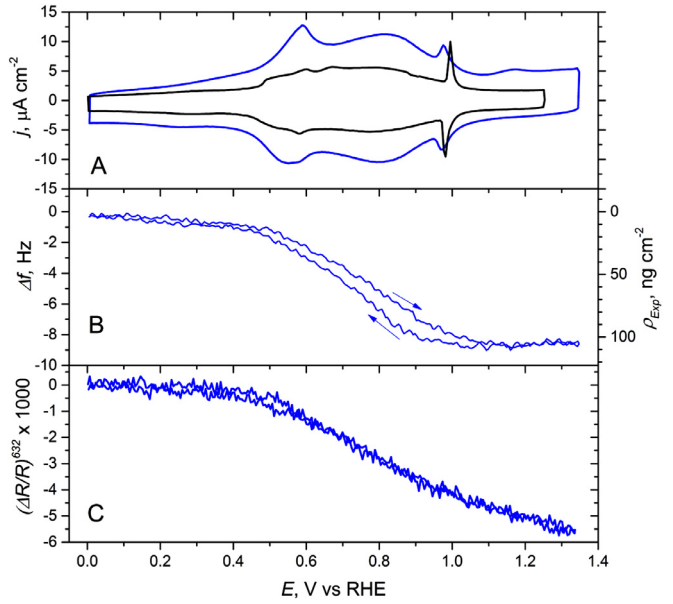

Fig. 11. Cyclic voltammogram (ν = 0.1 V/s, Panel A), averaged Δf (E_{Ref} = 0 V, 4 scans, Panel B), and $(\Delta R/R)^{632}$ (E_{ref} = 0.0 V, 27 scans, Panel C) vs. E, recorded simultaneously with a Au(111)-textured electrode 1 mM Na_2SeO_4 in 0.1 M $HClO_4$ (blue lines) as a function of E. Also included in Panel A is a voltammogram collected at ν = 0.05 V/s with a massive Au(111) single crystal in the same electrolyte (black line).

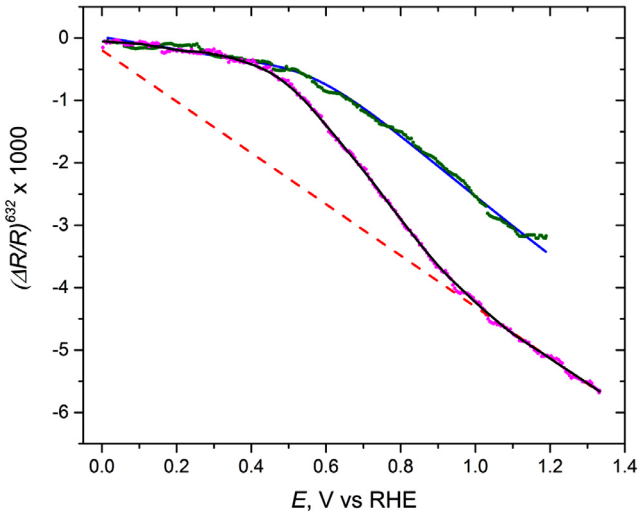

Fig. 12. Plot of $(\Delta R/R)^{632}$vs E for a Au(111)-textured electrode in 0.1 M $HClO_4$ (green line, average of 27 scans) and 0.1 M $HClO_4$ + 1 mM Na_2SeO_4 (magenta line, average of 27 scans) acquired at v = 0.1 V/s in the cathodic direction. The blue line represents the best fit of Eq. (3) to the data in 0.1 M $HClO_4$ (fit parameters in caption of Fig. 3), and the black line is the result of Lowess smoothing of the data collected in 0.1 M $HClO_4$ + 1 mM Na_2SeO_4. The dashed red line is the best linear fit to the magenta data in the range 1.0 V < E < 1.33 V, i.e. Best fit equation is $\Delta R/R$ = -4.11 E/V - 0.2.

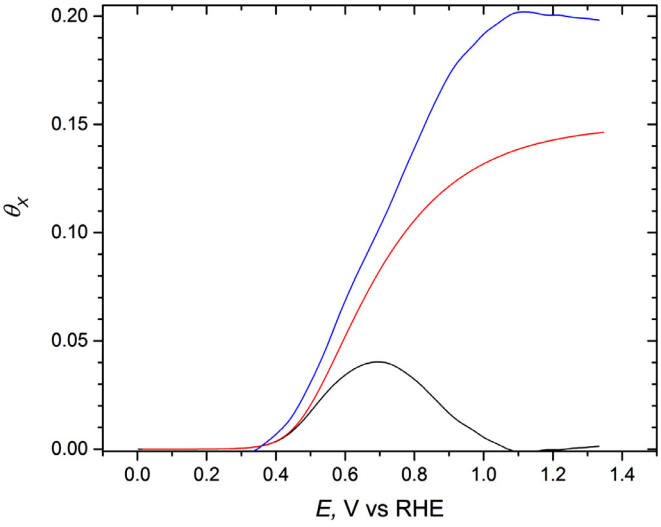

Fig. 13. Plots of $\theta^{mix}_{SeO_4^{2-}}$(blue line), $\theta^{mix}_{ClO_4^-}$ (black line) and $\theta_{ClO_4^-}$ (red line) as a function of the applied potential, calculated using the experimental data from Fig. 12 with Eqs (9) and (10) (see text for details).

are clearly much higher than this, even if referenced to the mass density at 0.45 V, i.e. just prior to anion adsorption. This larger mass can likely be attributed to the presence of co-adsorbed water. Nonetheless, if water does indeed co-adsorb with each anion, it most likely adopts an identical coverage for $SO_4^{2-}(ads)$ and $SeO_4^{2-}(ads)$, as the mass difference in the plateau regions for $SO_4^{2-}(ads)$ and $SeO_4^{2-}(ads)$, i.e. 20.4 ng/cm^2, is very close to the mass density difference between θ = 0.2 of Se and S, i.e. 21.6 ng/cm^2. On this basis, it will be assumed for all upcoming calculations that $\theta^{sat}_{SeO_4^{2-}} = \theta^{sat}_{SO_4^{2-}} = 0.2$. This common saturation coverage may not be surprising in view of the similar sizes of both oxyanions, as determined by large angle X-ray scattering (LAXS) experiments [19,20].

Shown in Fig. 11 is the cyclic voltammogram (ν = 0.1 V/s, black line, Panel A), and averaged Δf (Panel B), and $(\Delta R/R)^{632}$ (E_{ref} = 0.0 V, Panel C) vs. E, recorded simultaneously with a Au(111)-textured electrode in 0.1 M $HClO_4$ + 1 mM Na_2SeO_4, as a function of E.

The success of our primitive model in accounting for the optical data in the $ClO_4^-(aq)/SO_4^{2-}(aq)$ mixed electrolyte prompted us to apply it to determine the adsorption isotherm of $SeO_4^{2-}(aq)$ in 1 mM Na_2SeO_4 in 0.1 M $HClO_4$ solutions, for which no data appears to be available in the literature. In direct analogy with Eq. (6), application of the model would yield the following expression for $(\Delta R/R)^{632}_{mix}$

$$(\Delta R/R)^{632}_{mix} = (m_4E + b_4)\cdot\frac{\theta_{SeO_4^{2-}}}{\theta^{sat}_{SeO_4^{2-}}} + \left\{(m_1E + b_1)\frac{\theta_{ClO_4^-}}{\theta^{sat}_{ClO_4^-}} + (m_2E + b_2)\left(1 - \frac{\theta_{ClO_4^-}}{\theta^{sat}_{ClO_4^-}}\right)\right\} \times \left(1 - \frac{\theta_{SeO_4^{2-}}}{\theta^{sat}_{SeO_4^{2-}}}\right) \quad (9)$$

The terms $(\Delta R/R)^{632}_{mix}$ and $(\Delta R/R)^{632}$ (see term in curly brackets) in this equation are known (see black and blue lines in Fig. 12), and represent, respectively, the electroreflectance in 1 mM Na_2SeO_4 in 0.1 M $HClO_4$, and 0.1 M $HClO_4$ solutions, whereas, m_4, b_4 and $\theta_{SeO_4^{2-}}$ are unknown. However, m_4 and b_4 can be obtained by fitting a linear function to $(\Delta R/R)^{632}_{mix}$ vs E at potentials where the surface is saturated with $SeO_4^{2-}(ads)$ (dashed red line, Fig. 12). On this basis, it becomes possible to solve for $\theta_{SeO_4^{2-}}$as a function of E, by using the blue, black and red lines in Fig. 12. The coverage results obtained are shown in Fig. 13, alongside the coverage of co-adsorbed $ClO_4^-(aq)$, $\theta^{mix}_{ClO_4^-}$, calculated from Eq. (10), and $\theta_{ClO_4^-}$values determined by Zhumaev et al. in SeO_4^{2-}–free 0.1 M $HClO_4$ [7].

$$\theta^{mix}_{ClO_4^-} = \left(1 - \theta_{SeO_4^{2-}}/\theta^{sat}_{SeO_4^{2-}}\right)\times\theta_{ClO_4^-} \quad (10)$$

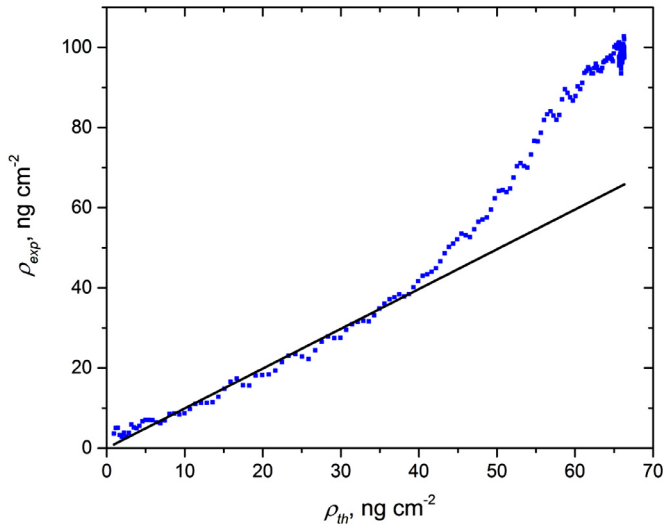

Fig. 14. Plot of the mass density measured via EQCM in 1 mM Na_2SeO_4 in 0.1 M $HClO_4$, ρ_{exp}, against the mass of $ClO_4^-(ads)$and $SO_4^{2-}(ads)$ calculated from Eq. (11), ρ_{th}, where $\rho_{exp}$was zeroed at the onset for anion adsorption, E = 0.35 V. The black line is a linear fit to the plot for $\rho_{exp} < 41$ ng/cm^2, which corresponds to 0.35 V < E < 0.7 V. The best fit function is $\rho_{exp} = 0.99 \times \rho_{th}$.

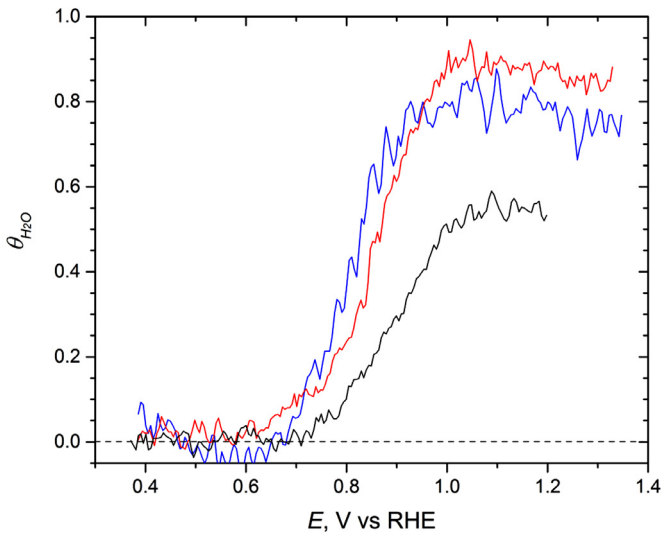

Fig. 15. Plot of the water coverage, θ_{H_2O}, vs E for a Au(111)-textured electrode in 0.1 M $HClO_4$ before (black line), and after adding either 1 mM Na_2SO_4 (red line) or 1 mM Na_2SeO_4 (blue line). Coverage was calculated as $(\rho_{exp} - \rho_{th})/(M_{H_2O} \cdot d_{Au(111)})$.

It becomes evident from these results that the onset of $SeO_4^{2-}(aq)$ adsorption occurs at a potential ca. 150 mV more negative than the corresponding value for $SO_4^{2-}(aq)$ and indeed similar to that for $ClO_4^-(aq)$ under the condition of these experiments. On this basis, it is not surprising that $\theta^{mix}_{ClO_4^-}$ is, overall, much lower than that observed in the case of the $ClO_4^-(aq)/SO_4^{2-}(aq)$ mixed electrolyte. In analogy with the microgravimetric data collected in the latter media, a linear correlation was found between the experimental mass density, ρ_{exp}, and the anion mass density predicted by our model, ρ_{th}, between the onset of anion adsorption (0.35 V) and E = 0.7 V determined from

$$\rho_{th} = (M_{ClO_4^-}\theta^{mix}_{ClO_4^-} + M_{SeO_4^{2-}}\theta_{SeO_4^{2-}}) \cdot d_{Au(111)} \quad (11)$$

up to ρ ca. 40 ng/cm^2, yielding a slope of 0.99 and a zero intercept (see Fig. 14). This behavior affords a strong indication that increase in ρ_{exp} measured within the specified range is exclusively due to the co-adsorption of $ClO_4^-(aq)$ and $SeO_4^{2-}(aq)$. As was found earlier, ρ_{exp} deviates markedly from linearity for higher ρ_{th} values.

3.4. Co-adsorption of water with perchlorate, selenate and sulfate on Au(111)

As clearly shown in Figs. 4, 8 and 14, for E < ca. 0.73 V vs RHE, the potential dependent increase in ρ_{exp} is essentially equal to the mass density increase anticipated for adsorption of fully desolvated anions, ρ_{th}. This somewhat unexpected correlation, could, in principle, be accounted for by assuming that the number of water molecules in the solvation sphere of the adsorbed anion is equal to the number being displaced by adsorption of the partially solvated anion. However, this was not the case for E > ca. 0.73 V, where ρ_{exp} was found to exceed ρ_{th}. In fact, the excess mass, i.e. $\rho_{exp} - \rho_{th}$, for adsorption of $ClO_4^-(aq)$, $SO_4^{2-}(aq)$and $SeO_4^{2-}(aq)$ at saturation coverages was equivalent to θ= 0.55, 0.86 and 0.80 of water molecules, which would yield, in each case, a nearest integer water to anion ratio of 4:1. SXS [18] and STM [13] studies at Au(111)/sulfuric acid solution interfaces have both firmly established that a single hydronium cation co-adsorbs with $SO_4^{2-}(aq)$ at saturation, and becomes incorporated into the ordered array of adsorbed anions on the electrode surface. Both SXS and STM are best suited for investigating rigid, ordered adlayers, and afford no insight for lower coverages where the adlayers are believed to be composed of more mobile adsorbates including water. Since EQCM allows us to assess the degree of hydration at any potential where anion coverages are known, we were able to demonstrate that the water/anion co-adsorption ratio varies with potential and the nature of the anion, reaching a fixed value only at saturation. In addition, the discrepancy between our water to anion ratio (4:1) and that reported by STM and SXS (1:1) may be due to some of the co-adsorbed water existing in a more mobile form not visible to STM and SXS.

Ataka and Osawa [9,10] investigated the co-adsorption of water with anions on Au(111) in both pure perchloric and sulfuric acid solutions by SEIRAS. In both cases, these authors reported IR bands ascribed to the OH stretching and HOH bending modes of surface water of negligible intensity from the onset of anion adsorption to ca. 0.76 V vs RHE. Above 0.76 V, however, the intensity of such spectral features were found to increase alongside that associated with the vibrational modes for $ClO_4^-(ads)$ and $SO_4^{2-}(ads)$. Although the solution composition in these studies was not identical to our own, the onset potential for the appearance of these water peaks was very close to the onset of excess mass measured by EQCM in this work, providing qualitative support for the assignment of $\rho_{exp} - \rho_{th}$ to water. Fig. 15 provides a quantitative measure of the coverage of water molecules as a function of the applied potential, not available from the spectroscopic measurements alone.

4. Conclusions

Analyses of data collected from simultaneous optical and gravimetric measurements presented in this work yielded quantitative information regarding co-adsorption of perchlorate, sulfate, selenate and water on Au(111)-textured electrodes from aqueous solutions as a function of the applied potential. The theoretical model employed, reported earlier in our laboratory, assumes the differential reflectance response arises from additive contributions from the bare and anion covered fractions of the electrode surface, and that the intrinsic reflectance of each fraction is linearly dependent on the potential. Relying on adsorption isotherms for perchlorate and sulfate determined by independent means, the reflectance for Au(111) in 0.1 M $HClO_4$ with and without 1 mM Na_2SO_4 were successfully fitted to the model. The results obtained in 1 mM Na_2SO_4

in 0.1 M $HClO_4$ afforded strong evidence for the co-adsorption of both anions over a significant potential range and for the full displacement of perchlorate by sulfate at much higher potentials. The model was then applied to measurements obtained in mixed 0.1 M $HClO_4$ + 1 mM Na_2SeO_4 electrolyte, whereby the gravimetric results were found to be consistent with a selenate saturation coverage virtually identical to that found for sulfate in 1 mM Na_2SO_4 in 0.1 M $HClO_4$, i.e. 0.2. On this basis, it became possible to obtain for the first time an adsorption isotherm for selenate under the conditions of these experiments. Finally, the mass density increases derived from anion coverages were found to be roughly equal to their experimental equivalents measured by EQCM for $E <$ ca. 0.73 V in all three solutions. Above this potential threshold, experimental masses were larger than the masses anticipated for anions alone, an effect attributed to water co-adsorption. The water to anion co-adsorption ratio was found to be around 4:1 for the highest potentials in each solution.

Declaration of Competing Interest

The authors declare that they have no known competing financial interests or personal relationships that could have appeared to influence the work reported in this paper.

Declaration of Competing Interest

The authors declare no conflict of interest.

Credit authorship contribution statement

Jonathan R. Strobl: Conceptualization, Methodology, Software, Writing – original draft, Writing – review & editing. **Daniel Scherson:** Conceptualization, Methodology, Writing – review & editing.

Acknowledgments

This work was supported by a grant from NSF, CHE-1808592.

References

[1] A.J.J. Jebaraj, D.A. Scherson, Quantitative aspects of normalized differential reflectance spectroscopy: Pt(111) in aqueous electrolytes, Anal. Chem. 86 (2014) 4241–4248.
[2] J. Xu, D. Scherson, Quantitative correlations between the normal incidence differential reflectance and the coverage of adsorbed bromide on a polycrystalline platinum rotating disk electrode, Anal. Chem. 85 (2013) 2795–2801.
[3] I. Fromondi, F. Zhu, D.A. Scherson, *In situ* spectroscopy at the quasi-perfect Pt(111) single-crystal facet|aqueous electrolyte interface, J. Phys. Chem. C 116 (2012) 19613–19624.
[4] D.M. Kolb, UV-visible reflectance spectroscopy, in: R.J. Gale (Ed.), Spectroelectrochemistry Theory and Practice, Springer US, New York, 1988, pp. 87–188.
[5] J.R. Strobl, D.A. Scherson, The reduction of selenate mediated by underpotential deposited copper on gold electrodes in acidic solutions: analytical applications, J. Electrochem. Soc. 163 (2016) H1066–H1068.
[6] Y. Mo, E. Hwang, D.A. Scherson, Simultaneous normalized optical reflectivity and microgravimetric measurements at electrode/electrolyte interfaces: the adsorption of bromide on gold in aqueous media, Anal. Chem. (1995) 2415–2418.
[7] U.M. Zhumaev, A.S. Lai, I.V. Pobelov, A. Kuzume, A.V. Rudnev, T. Wandlowski, Quantifying perchlorate adsorption on Au(111) electrodes, Electrochim. Acta 146 (2014) 112–118.
[8] Z. Shi, J. Lipkowski, M. Gamboa, P. Zelenay, A. Wieckowski, Investigations of SO_4^{2-} adsorption at the Au(111) electrode by chronocoulometry and radiochemistry, J. Electroanal. Chem. 366 (1994) 317–326.
[9] K.I. Ataka, T. Yotsuyanagi, M. Osawa, Potential-dependent reorientation of water molecules at an electrode/electrolyte interface studied by surface-enhanced infrared absorption spectroscopy, J. Phys. Chem. 100 (1996) 10664–10672.
[10] K.I. Ataka, M. Osawa, *In situ* infrared study of water-sulfate coadsorption on gold(111) in sulfuric acid solutions, Langmuir 14 (1998) 951–959.
[11] K.A. Gruebel, J.A. Davis, J.O. Leckie, Kinetics of oxidation of selenite to selenate in the presence of oxygen, Titania and light, Environ. Sci. Technol. 29 (1995) 586–594.
[12] S. Gong, J. Lu, H. Yan, Developing the self-contained hydrogen reference electrode, J. Electroanal. Chem. 436 (1997) 291–293.
[13] G.J. Edens, X. Gao, M.J. Weaver, The adsorption of sulfate on gold(111) in acidic aqueous media: adlayer structural inferences from infrared spectroscopy and scanning tunneling microscopy, J. Electroanl. Chem. 375 (1993) 357–366.
[14] Z. Shi, J. Lipkowski, S. Mirwald, B. Pettinger, Electrochemical and second harmonic generation study of SO_4^{2-} adsorption at the Au(111) electrode, J. Electroanal. Chem. 396 (1995) 115–124.
[15] O.M. Magnussen, J. Hagebok, J. Hotlos, R.J. Behm, *In situ* scanning tunneling microscopy observations of a disorder-order phase transition in hydrogensulfate adlayers on Au(111), Faraday Discuss. 94 (1992) 329–338.
[16] A. Cuesta, M. Kleinart, D.M. Kolb, The adsorption of sulfate and phosphate on Au(111) and Au(100) electrodes: an *in situ* STM study, Phys. Chem. Chem. Phys. 2 (2000) 5684–5690.
[17] I.R. de Moraes, F.C. Nart, Sulfate ions adsorbed on Au(hkl) electrodes: *in situ* vibrational spectroscopy, J. Electroanal. Chem. 461 (1999) 110–120.
[18] T. Kondo, J. Morita, K. Hanaoka, S. Takakusagi, K. Tamura, M. Takahasi, J. Mizuki, K. Uosaki, Structure of Au(111) and Au(100) single-crystal electrode surfaces at various potentials in sulfuric acid solution determined by *in situ* surface X-ray scattering, J. Phys. Chem. 111 (2007) 13197–13204.
[19] V. Vchirawongkwin, B.M. Rode, I. Persson, Structure and dynamics of sulfate ion in aqueous solution - an ab initio QMCF MD simulation and large angle X-ray scattering study, J. Phys. Chem. B 111 (2007) 4150–4155.
[20] L. Eklund, I. Persson, Structure and bonding of the hydrated selenite and selenate ions in aqueous solutions, Dalton Trans. 43 (2014) 6315–6321.